

Lawrence Berkeley National Laboratory

LBL Publications

Title

Molybdenum Disulfide Catalytic Coatings via Atomic Layer Deposition for Solar Hydrogen Production from Copper Gallium Diselenide Photocathodes

Permalink

<https://escholarship.org/uc/item/8zt9q9vj>

Journal

ACS Applied Energy Materials, 2(2)

ISSN

2574-0962

Authors

Hellstern, Thomas R
Palm, David W
Carter, James
[et al.](#)

Publication Date

2019-02-25

DOI

10.1021/acsaem.8b01562

Peer reviewed

¹Molybdenum Disulfide Catalytic Coatings
²via Atomic Layer Deposition for Solar
³Hydrogen Production from Copper
⁴Gallium Diselenide Photocathodes

⁵*Thomas R. Hellstern, David W. Palm, James Carter, Alex D. DeAngelis,*

⁶*Kimberly Horsley, Lothar Weinhardt, Wanli Yang, Monika Blum, Nicolas*

⁷*Gaillard, Clemens Heske, Thomas F. Jaramillo**

⁸Dr. T.R. Hellstern, D.W. Palm, Prof. T.F. Jaramillo*

⁹Department of Chemical Engineering, Stanford University
¹⁰443 Via Ortega, Stanford, California 94305, United States

¹¹

¹²J. Carter, Dr. L. Weinhardt, Dr. M. Blum, Prof. C. Heske

¹³Department of Chemistry and Biochemistry, University of Nevada Las Vegas
¹⁴(UNLV)

¹⁵4505 Maryland Pkwy, Las Vegas, Nevada 89154-4003, United States

¹⁶

¹⁷A.D. DeAngelis, Dr. K. Horsley, Dr. N. Gaillard

¹⁸Hawaii Natural Energy Institute (HNEI), University of Hawaii at Manoa

¹⁹1680 East-West Rd, POST 109, Honolulu, Hawaii 96822, United States

²⁰

²¹Dr. L. Weinhardt, Prof. C. Heske

²²Institute for Photon Science and Synchrotron Radiation (IPS), Karlsruhe

²³Institute of Technology (KIT)

²⁴Hermann-v.-Helmholtz-Platz 1, 76344 Eggenstein-Leopoldshafen, Germany

²⁵

²⁶Institute for Chemical Technology and Polymer Chemistry (ITCP), Karlsruhe

²⁷Institute of Technology (KIT)

28Engesserstr. 18/20, 76128 Karlsruhe, Germany

29

30Dr. W. Yang, Dr. M. Blum

31Advanced Light Source (ALS), Lawrence Berkeley National Laboratory

321 Cyclotron Road, Berkeley, California 94720, United States

33

34Prof. T.F. Jaramillo*

35SUNCAT Center for Interface Science and Catalysis, SLAC National

36Accelerator Laboratory

372575 Sand Hill Road, Menlo Park, California 94025, United States

38

39*Corresponding Author: jaramillo@stanford.edu

40

41KEYWORDS: Photoelectrochemical water splitting, copper gallium diselenide,

42molybdenum disulfide, hydrogen evolution, atomic layer deposition

43

44 ABSTRACT: We demonstrate that applying atomic layer deposition-

45derived molybdenum disulfide (MoS_2) catalytic coatings on copper gallium

46diselenide (CGSe) thin film absorbers can lead to efficient wide band gap

47photocathodes for photoelectrochemical hydrogen production. We have

48prepared a device that is free of precious metals, employing a CGSe

49absorber and a cadmium sulfide (CdS) buffer layer, a titanium dioxide (TiO_2)

50interfacial layer, and a MoS_2 catalytic layer. The resulting

51 $\text{MoS}_2/\text{TiO}_2/\text{CdS}/\text{CGSe}$ photocathode exhibits a photocurrent onset of +0.53 V

52vs. RHE and a saturation photocurrent density of -10 mA cm^{-2} , with stable

53operation for greater than 5 hours in acidic electrolyte. Spectroscopic

54investigations of this device architecture indicate that overlayer degradation

55occurs inhomogeneously, ultimately exposing the underlying CGSe absorber.

56Introduction

57 Hydrogen is an extremely important commodity chemical, used
58 primarily for ammonia synthesis and hydrocarbon upgrading. It is produced
59 on a scale of 65 million metric tons per year.^{1,2} Steam reforming of natural
60 gas is currently the dominant industrial source of hydrogen, although it emits
61 the greenhouse gas CO₂ as a byproduct. Thus, more sustainable hydrogen
62 production methods have the potential to substantially reduce greenhouse
63 gas emissions.³ In contrast, photoelectrochemical (PEC) water splitting,
64 which uses sunlight and water to produce hydrogen and oxygen, offers a
65 promising route for producing hydrogen without the direct emission of CO₂.⁴⁻⁶
66 However, single-absorber PEC water splitting devices have not demonstrated
67 suitable energy conversion efficiencies. Accordingly, numerous studies have
68 recommended the use of stacked dual-absorber PEC water splitting devices,
69 because this configuration can achieve higher solar-to-hydrogen (STH)
70 efficiencies.⁶⁻¹⁰

71 A key challenge in implementing an efficient dual-absorber PEC water
72 splitting device is the development of a wide band gap photoelectrode that
73 (1) has a band gap between 1.6 and 1.8 eV, optimal for current and voltage
74 output to split water when paired with a smaller band gap photoelectrode,
75 and (2) maintains long-term, stable operation.^{5,11} The copper indium gallium
76 diselenide (CuIn_{1-x}Ga_xSe₂ or CIGSe) chalcopyrite system contains promising
77 candidates for photoabsorbers due to high demonstrated photovoltaic
78 conversion efficiency,^{12,13} low-cost deposition methods,^{14, 15} and a
79 compositionally-tunable band gap.¹⁶

80 Copper gallium diselenide (CuGaSe_2 or CGSe) has the widest band gap
81 (~1.7 eV) of the CIGSe material class and has been previously used as a p-
82 type absorber in PEC systems.¹⁷⁻²⁰ However, the CGSe band edges do not
83 align with the hydrogen and oxygen evolution redox potentials, which leads
84 to a poor onset potential for the hydrogen evolution reaction (HER).¹⁹ In order
85 to overcome this limitation, cadmium sulfide (CdS) has been employed as a
86 buffer layer to improve the photovoltage and therefore the onset potential
87 for HER.^{17,18,21} Unfortunately, CdS has been shown to be highly unstable
88 under illumination in aqueous conditions.^{22,23} Although work has been done
89 on the durability of CdS/CGSe electrodes in neutral conditions, operation of a
90 water splitting device at pH = 7 may introduce additional challenges due to
91 the formation of pH gradients.^{18,24} Hence, there is incentive to develop
92 catalytic schemes that extend the operation of CdS/CGSe for splitting water
93 in acidic or basic electrolyte.

94 Molybdenum sulfides are promising catalytic layers for CdS/CGSe for
95 several reasons. MoS_2 thin films have demonstrated excellent stability in
96 acidic electrolytes and have enhanced the durability of silicon and III-V
97 semiconductor photocathodes.²⁵⁻³⁰ The edge sites of MoS_2 are also some of
98 the most active non-precious-metal hydrogen evolution catalyst sites, on a
99 turnover frequency basis.^{31,32} To date, MoS_2 catalytic layers for
100 photoelectrodes have only been formed from sputtered films of molybdenum
101 or by electrodeposition. We have developed a new method to deposit
102 extremely thin, low light absorbing MoS_2 -based schemes via low temperature

103atomic layer deposition (ALD). Here, we report on their activity, durability,
104and degradation mechanisms when integrated with CdS/CGSe
105photoelectrodes.

106 In particular: (1) we have integrated thin films of MoS₂ and TiO₂
107deposited via ALD to serve as a catalytic scheme for polycrystalline, rough
108films of CdS/CGSe. (2) We have investigated the electrochemical activity and
109durability of the resulting MoS₂/TiO₂/CdS/CGSe photocathode. (3) We have
110performed soft x-ray spectroscopy to gain insight into the degradation
111mechanisms of the MoS₂/TiO₂/CdS/CGSe photocathode.

112**Experimental Methods**

113*Device Fabrication*

114 CGSe films were deposited on clean soda-lime glass coated with 400
115nm of fluorine-doped tin oxide (FTO substrates, Hartford City Glass, TEC 15,
11615 Ω/sq.). FTO substrates were cleaned by sonicating them inalconox
117solution (2 wt. %), acetone, then methanol, each for 5 minutes. Substrates
118were thoroughly rinsed in de-ionized (DI) water between each sonication
119step. The films were deposited by a three-stage co-evaporation process³³
120modified to yield CuGaSe₂, which has been shown to make a good ohmic
121contact to the FTO.³⁴ In the first stage, gallium (1.5 Å/s) and selenium (20.0
122Å/s) were co-evaporated onto the substrates at a nominal substrate
123temperature (T_{sub}) of 420°C. In the second stage, copper (1.0 Å/s) and
124selenium were deposited at a T_{sub} of 580°C. Copper continued to be
125deposited such that a decrease in temperature of 3-10°C occurred after end

126point detection (EPD). In the third stage, gallium and selenium were
127deposited once more until the substrate temperature increased back to its
128initial value prior to EPD. The thickness of copper and gallium was monitored
129during the deposition by an electron impact emission spectrometer
130(Guardian EIES controller, Inficon). The thickness of the CGSe films for this
131study was approximately 1 μm , as measured by a stylus profilometer (Alpha
132step 200, Tencor).

133 Cadmium sulfide (CdS) was deposited on CGSe by chemical bath
134deposition (CBD), following the recipe described in Ref. 22. In short, a 50 mL
135CBD solution was made in a reaction vessel containing 5 mL of 1.5 M
136cadmium sulfate 8/3 hydrate (Sigma) solution, 6.25 mL of 30% ammonium
137hydroxide solution (Fisher), 2.5 mL of 1.5 M thiourea (Sigma) solution, and
13836.25 mL of DI water. The vessel was heated to 65°C by placing it into a
139recirculating water bath that was preheated to this temperature. CGSe
140samples were suspended in the reaction vessel, and the reaction was
141allowed to proceed for 10-12 minutes. Samples were removed, washed in DI
142water, and dried immediately with air before transporting to a cleanroom
143environment for further deposition. Cadmium sulfide is toxic and cadmium
144compounds are known carcinogens; as such, all CdS depositions were
145performed in a specified area in a fume hood, and all waste created in the
146process was handled and stored separately from other laboratory waste.

147 TiO_2 was deposited using ALD as previously described,³⁵ using
148tetrakis(dimethylamido)titanium(IV) (TDMA-Ti) from Strem and DI water as

149precursors in a Cambridge Nanotech Savannah ALD reactor at 150°C.
150Saturated linear growth was observed with a growth rate of 0.45 - 0.50
151Å/cycle. The TDMA-Ti precursor was heated to 75°C for deposition and 5 nm
152of TiO₂ was deposited over 100 cycles. After TiO₂ deposition, the sample was
153transferred directly to the next ALD reactor for MoO_x deposition.

154 MoO_x was deposited using ALD parameters adapted from previous
155reports.³⁶ Unlike in previous studies, MoO_x was deposited using molybdenum
156hexacarbonyl (Mo(CO)₆) and oxygen plasma in a Cambridge Nanotech Fiji
157ALD reactor at 165°C. Saturated linear growth was observed with a growth
158rate of nearly 0.6 Å/cycle, as shown in **Figure S1**. The Mo(CO)₆ precursor
159was heated to 70°C for deposition and 4.5 nm of MoO_x was deposited over
16075 cycles. After MoO_x deposition, the sample was transferred back to our
161wet-chemistry laboratory for tube furnace annealing (see below). The
162thicknesses of the TiO₂ and MoO_x layers were determined using
163spectroscopic ellipsometry.

164 MoS₂ was synthesized by converting MoO_x under flowing 10% H₂S /
16590% H₂ (approx. 10 sccm) in a tube furnace at 200°C for 30 minutes.³⁷ The
166furnace was heated to 200°C while samples were held outside of the
167temperature zone (at ~30°C). Samples were then inserted into the
168temperature zone, subsequently reaching 200°C over the course of 3.5
169minutes. After 30 minutes, samples were removed from the temperature
170zone and allowed to rapidly cool. Hydrogen sulfide (H₂S) is a highly toxic and

171flammable gas, which must only be used and stored inside a ventilated fume
172hood. We test for H₂S leaks in our tube furnace setup using an RKI
173Instruments GX-2009 Portable Multi Gas Detector and scrub the effluent gas
174(forming CuS) using a glass bubbler containing aqueous hydrogen peroxide
175solution (30%) and copper wire.

176

177*Spectroscopic and Microscopic characterization*

178 X-ray Photoelectron Spectroscopy (XPS) and X-ray excited Auger
179Electron Spectroscopy (XAES) were performed at UNLV using a modified VG
180ESCALab MkII with a SPECS PHOIBOS 150 MCD electron analyzer and a
181SPECS XR-50 dual anode X-ray source. Sulfur L_{2,3} X-ray Emission
182Spectroscopy (XES) data was obtained at Beamline 8.0.1 of the Advanced
183Light Source (ALS), Lawrence Berkeley National Laboratory, using the newly
184installed iRIXS endstation (8.0.1.1).³⁸ After preparation and testing at
185Stanford, the samples were packaged in a dry nitrogen environment and
186transferred to UNLV. The packaging was opened in an N₂-filled glove box,
187and samples were mounted and transferred into ultra-high vacuum (UHV)
188without air exposure. For subsequent measurements at the ALS, the samples
189were repackaged in the glove box and transferred to the ALS in Berkeley.
190Some samples were directly transferred from Stanford to the ALS. Before
191transfer into the iRIXS chamber at the ALS, samples were briefly (< 5 min)
192exposed to air.

193 SEM was performed using a FEI Magellan 400 XHR at the Stanford
194Nano Shared Facility (SNSF). Optical transmission measurements were
195performed using a Varian Cary 6000i UV-Vis-NIR spectrophotometer at the
196Stanford Soft Materials Facility (SMF). Optical absorption measurements were
197performed using an integrating sphere with white light from a 1000 W xenon
198lamp. Light was directed onto the sample and unabsorbed light was collected
199and measured using an Ocean Optics Jaz EL 200-XR1 spectrometer. X-ray
200diffraction measurements were performed using a Philips PANalytical X'Pert
201Pro in parallel beam mode with Cu K α radiation.

202*Photoelectrochemical Characterization*

203 The CdS/CGSe photocathodes were prepared by first physically
204removing part of the CGSe film from the FTO substrate using a razor blade
205and then making electrical contact to the exposed FTO using conductive
206carbon paint (DAG-T-502). A tinned copper insulated hookup wire (Belden
2078502-009) was attached using the carbon paint, which was then allowed to
208dry for 10 minutes. The electrodes were mounted using inert epoxy (Loctite
209Hysol 9462) and allowed to cure overnight before testing. The active area of
210each sample was measured using a photograph and image analysis software
211(ImageJ); measured working electrode areas ranged from 0.15 to 0.3 cm².

212 PEC measurements³⁹ were performed in a three-electrode cell
213configuration using a Bio-Logic potentiostat (VSP) and a two-compartment
214glass cell separated by a proton-conducting Nafion membrane. The
215CdS/CGSe working electrode and Hg/Hg₂SO₄ (saturated K₂SO₄) reference

216electrode were placed in one compartment, while an IrO_x/Ir wire counter
217electrode was placed in the other compartment to minimize contamination.
218The front of the working electrode was illuminated through a fused silica
219window. In order to dissolve hydrogen gas and displace dissolved oxygen,
220the working electrode compartment was purged with H₂ for at least 10
221minutes prior to the cyclic voltammetry measurements, and during the
222course of the 24 hr chronoamperometry (CA) stability measurements. The
223reference electrode was calibrated to the reversible hydrogen electrode
224(RHE) scale by measuring the redox potential for the H⁺/H₂ couple using
225platinum working and counter electrodes in H₂-purged 0.5 M H₂SO₄
226electrolyte.

227 The performance of the CdS/CGSe photocathodes was assessed by
228performing linear sweep voltammetry (LSV) from -0.55 V vs. RHE to
229approximately 0.2 V positive of the onset potential at 10 mV s⁻¹. The onset
230potentials reported in this study were determined by a linear extrapolation of
231the LSV's main photocurrent onset feature to its intersection with the $j = 0$
232axis. The potential at which this intersection occurs is defined as the onset
233potential for the purposes of this study, similar to previously reported
234methods.³⁴ A graphical demonstration of this procedure is included in **Figure**
235**S2**. The stability of the CdS/CGSe photocathode was assessed by performing
236(1) an initial illuminated LSV, in the potential range described above, (2) a
237dark LSV between 0.0 V and -0.55 V vs. RHE at 10 mV s⁻¹, (3) a CA

238 measurement held at 0.0 V vs. RHE for 24 hrs, and (4), (5) final illuminated
239 and dark LSVs, respectively.

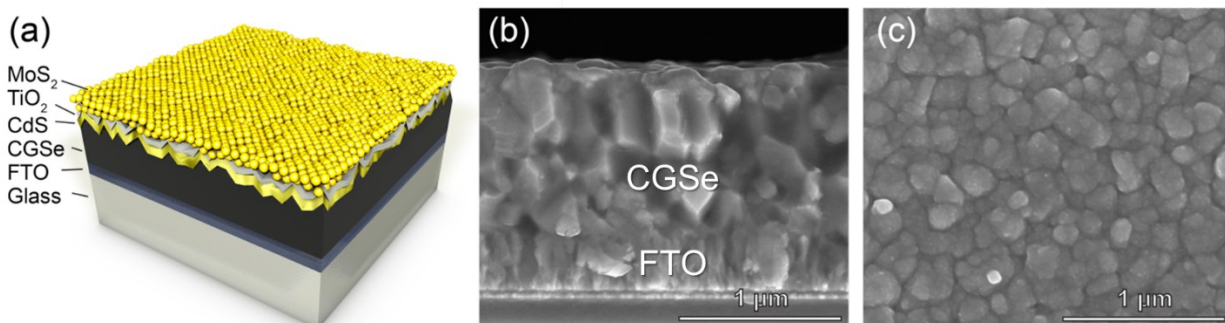
240 The light source used for 1-Sun PEC testing was a 150 W Xe arc lamp.
241 The irradiance was measured using an Ocean Optics Jaz EL 200-XR1
242 spectrometer and calibrated to match the AM1.5G solar spectrum. Details
243 about the calibration procedure are described in the supporting information.
244 The light source used for incident photon-to-current conversion efficiency
245 (IPCE) measurements was a 1000 W Hg/Xe arc lamp, in conjunction with a
246 Newport Oriel 74100 monochromator. The spectral output of the
247 lamp/monochromator assembly was measured using the Ocean Optics Jaz
248 spectrometer listed above.

249

250 **Results and Discussion**

251 *Synthesis of MoS₂/TiO₂/CdS/CGSe photocathodes*

252 A schematic diagram and SEM images of a
253 MoS₂/TiO₂/CdS/CGSe/FTO/glass photocathode are shown in **Figure 1**. X-ray
254 diffraction of CGSe electrodes, as shown in **Figure S3**, confirms the
255 chalcopyrite crystal phase. An FTO substrate was used to ensure optical
256 transmission of below band gap photons (Figure S4), an important quality for
257 creating a stacked tandem PEC water splitting device.



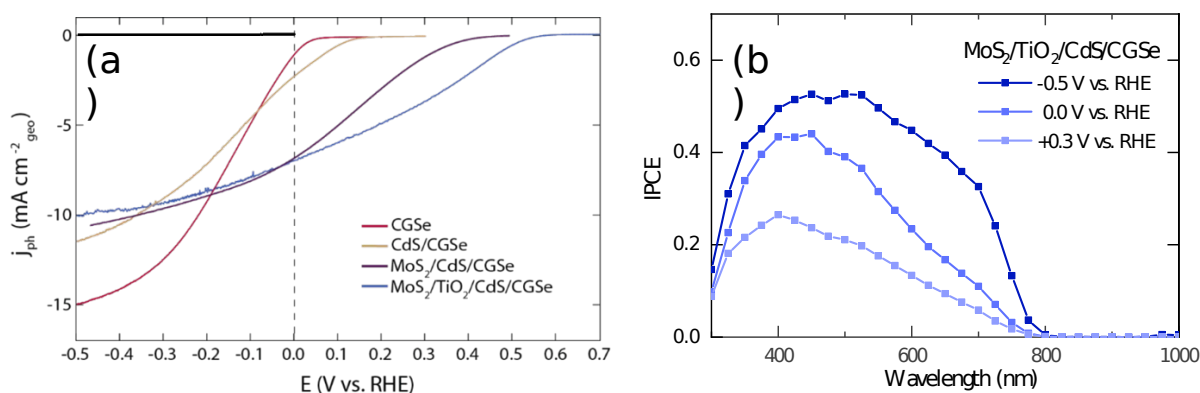
258

259 **Figure 1:** (a) Schematic, (b) cross-sectional SEM image, and (c) top view
 260 SEM image of MoS₂/TiO₂/CdS/CGSe photocathode on FTO. MoS₂, TiO₂, and
 261 CdS layers are thin and cannot be distinguished in the cross-section. SEM
 262 images also show the grain size distribution of CGSe.

263

264 As shown in **Figure 2a**, the best photocurrent onset was achieved
 265 when the buffer and both the MoS₂ and TiO₂ layers were included. The onset
 266 potential for the bare CGSe electrode was found at only +0.02 V vs. RHE,
 267 likely due to poor band alignment relative to the reversible hydrogen
 268 potential.¹⁹ In order to overcome the limitations of the CGSe-electrolyte
 269 junction, a CdS buffer layer was deposited by CBD to create a solid-state
 270 junction analogous to those widely used in CIGSe photovoltaic devices.^{21,40}
 271 With the addition of CdS, the onset improved to +0.12 V vs. RHE, a modest
 272 increase with room for improvement since CdS is a poor catalyst for HER. The
 273 onset was further improved by the addition of a MoS₂ catalytic layer,
 274 reaching +0.35 V vs. RHE. Furthermore, the treatment time and temperature
 275 utilized during the formation of MoS₂ from MoO_x in sulfurous atmosphere
 276 were optimized for catalytic performance, transparency, and durability, and
 277 utilizing TiO₂ as an additional interfacial layer demonstrated further
 278 enhanced performance (**Figures S5-7**). This optimized MoS₂/TiO₂/CdS/CGSe

279 photocathode showed an onset of +0.53 V vs. RHE and achieved a
 280 photocurrent density of -10 mA cm^{-2} at -0.5 V vs. RHE (Figure 2a). In addition,
 281 a maximum IPCE of 0.53 was achieved for this device under bias of -0.5 V vs.
 282 RHE and a maximum IPCE of 0.44 was achieved at 0 V vs. RHE (**Figure 2b**).



283

284 **Figure 2:** (a) PEC activity of the bare CGSe (red), CdS/CGSe (gold),
 285 MoS₂/CdS/CGSe (purple), and MoS₂/TiO₂/CdS/CGSe (blue) samples tested
 286 under AM1.5G illumination; the dark LSV for the MoS₂/CdS/CGSe sample
 287 (typical of all samples) is shown in black for reference. (b) Incident photon-
 288 to-current conversion efficiency (IPCE) of the MoS₂/TiO₂/CdS/CGSe device at
 289 various applied potentials. All electrodes were tested in H₂-sparged 0.5 M
 290 H₂SO₄ electrolyte with a Hg/HgSO₄ reference electrode and an Ir/IrO_x counter
 291 electrode.

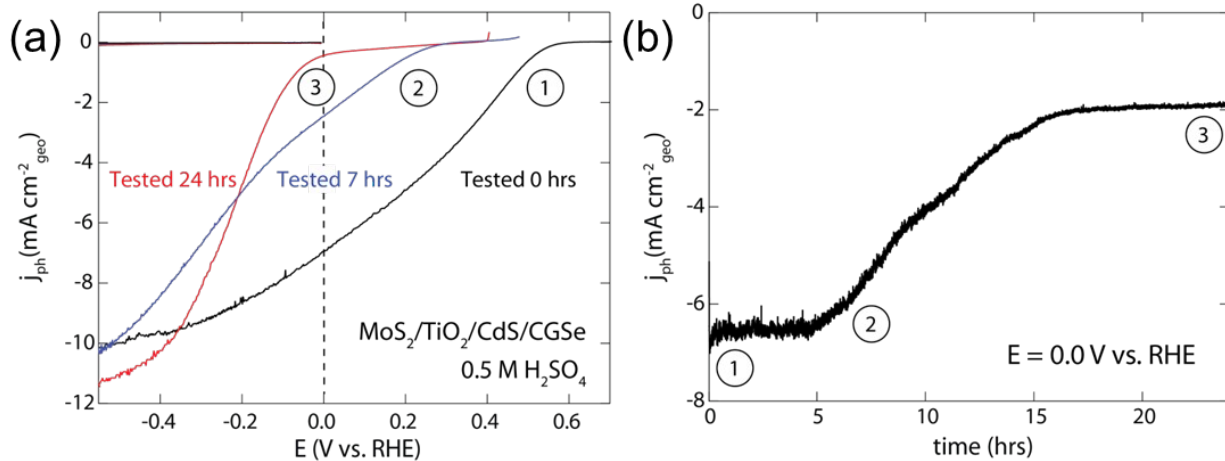
292

293 *Assessing the durability of MoS₂/TiO₂/CdS/CGSe photocathodes*

294 In order to evaluate PEC durability of the MoS₂/TiO₂/CdS/CGSe
 295 photocathode, CA tests were conducted in which the potential was
 296 maintained at 0 V vs. RHE for 24 hrs under constant illumination, with LSVs
 297 were performed at 0 and 24 hrs. Hydrogen production is the dominant
 298 contributor to the photocurrent generated over the course of the experiment,
 299 given the sustained bubble formation at the electrode surface, the
 300 substantial total charge passed (10^{-3} mol e^- , calculated in the Supporting

301Information), and the well-documented high Faradaic efficiencies for H₂
302evolution on MoS₂ catalysts.²⁹ An identically-prepared sample was tested in
303this manner for 7 hrs and then characterized to gain insight into the
304chemical changes occurring at the photocathode surface over the course of
305electrochemical testing. **Figure 3** shows (a) LSVs at 0, 7, and 24 hr time
306intervals, and (b) CA stability data (at 0.0 V vs. RHE) over 24 hrs.

307 During the LSVs in **Figure 3a**, this MoS₂/TiO₂/CdS/CGSe photocathode
308tested at 0 hrs showed an onset potential of +0.53 V vs. RHE, and achieved
309an approximate saturation photocurrent density of -10 mA cm⁻²; the
310maximum dark current over the measured potential range was -0.02 mA cm⁻²
311(Figure 3a). After 7 hrs of testing, the onset potential shifted to +0.25 V vs.
312RHE, with the shape of the LSV changing significantly. After 24 hrs of testing,
313the onset potential shifted to -0.05 V vs. RHE and the shape of the curve
314again changed substantially to resemble that of the bare CGSe electrode
315shown in Figure 2. The saturation photocurrent density of the electrode also
316increased after 24 hrs of testing, consistent with a thinning of the CdS layer,
317which parasitically absorbs incident light (**Figure S7**). The CA measurement
318in **Figure 3b** indicates that the electrode current density is stable for
319approximately 5 hrs at -6.5 mA cm⁻², before degrading to -2 mA cm⁻² after 15
320hrs. The maximum dark current increases steadily to a final value of -0.09
321mA cm⁻² after 24 hrs of durability testing, as shown in Figure S8.



322

323 **Figure 3:** (a) LSVs of MoS₂/TiO₂/CdS/CGSe photocathodes as prepared
 324 (black), after 7 hrs stability testing (blue), and after 24 hrs of stability testing
 325 (red). The corresponding dark scans are also shown. (b) A 24 hr stability test
 326 tracking the current density at 0.0 V vs. RHE. LSV time points from (a) are
 327 marked (1-3). Tests performed under simulated AM1.5G illumination.

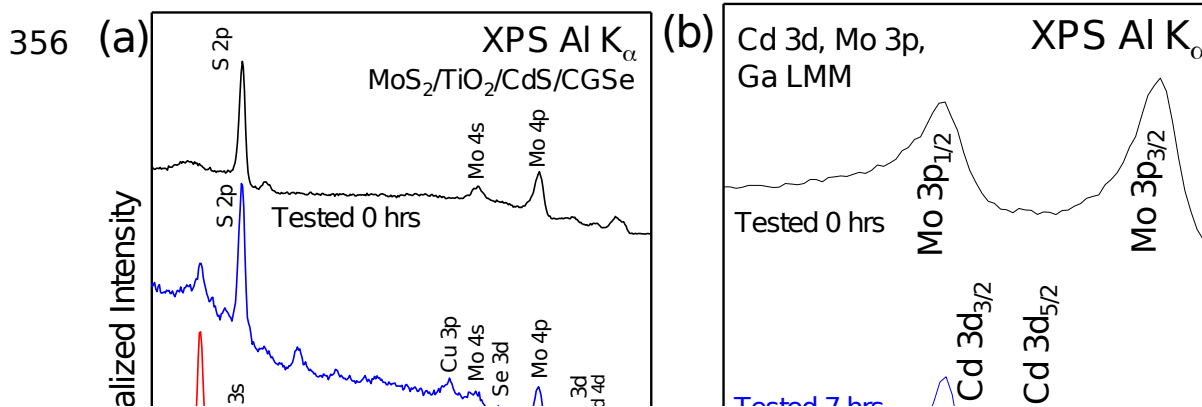
328

329 *Spectroscopic investigation of degradation in MoS₂/TiO₂/CdS/CGSe*
 330 *photocathodes*

331 We performed spectroscopic studies of the as-prepared and tested
 332 photoelectrodes and combined this information with the preceding
 333 photoelectrochemical data in order to understand the device degradation.
 334 From this combination of techniques, it is evident that significant changes in
 335 surface composition occurred during the testing process. We postulate that
 336 device deterioration occurs as the electrolyte infiltrates and dissolves the
 337 MoS₂/TiO₂ films and the underlying CdS due to instabilities in acidic media.

338 **Figure 4a** shows an XPS survey of the shallow core levels, while
 339 **Figures 4b, 4c,** and **4d** depict the Cd 3d/Mo 3p/Ga LMM XPS and XAES
 340 spectra, the Ti 2p XPS spectra, and the S L_{2,3} XES spectra, respectively. The
 341 surface-sensitive XPS spectra (Figures 4a-c) show that the as-prepared

342sample surface (“Tested 0 hrs”) was dominated by the MoS₂/TiO₂ dual layer,
 343while the sample surface after 7 hrs of testing exhibits a mixture of chemical
 344environments, showing strong characteristic peaks for S, Cd, and Mo, as well
 345as weaker signals for Ti, Cu, Se, and Ga. After 24 hours of testing, the XPS
 346signals primarily resemble those of a CGSe surface. Furthermore, the S L_{2,3}
 347XES spectra (Figure 4d), with significantly larger attenuation depth, show the
 348presence of a CdS chemical environment in the film (in particular the Cd 4d-
 349derived peaks^{41,42} labeled (b)) for the 0 and 7 hrs-tested samples. In
 350comparison to the CdS reference, the upper valence band feature labeled (c)
 351shows a slightly more symmetric spectral shape and is shifted to higher
 352emission energies, possibly indicative of spectral contributions from S in a
 353MoS₂ chemical environment. In contrast, the S signal is completely removed
 354after 24 hours of testing, and only a broad Se M_{2,3} peak at 148 eV is
 355observed.⁴³



357 We posit that, during the degradation processes, the surface of the
 358electrode was composed of regions of MoS₂/TiO₂, exposed CdS, as well as
 359bare CGSe. This model agrees with the XPS data taken at 7 hrs (Figures 4a

360and 4c) and the LSV after 7 hrs of testing in Figure 3a, where the more
361positive onset potential compared to that of the bare CGSe (Figure 2) is
362evidence that some portion of the CdS/CGSe junction and the associated
363catalytic overlayers remained intact. This suggests that the degradation
364process is inhomogeneous and may involve multiple mechanisms. After 24
365hrs of testing, significant degradation of the overlayers had occurred, as
366evidenced by the similarity of both the LSV and spectroscopic scans to those
367of the bare CGSe absorber electrode, with similar onset potential but slightly
368lower saturation photocurrent density.

369

370**Conclusions**

371 A low-temperature scheme ($< 200^{\circ}\text{C}$) was developed using ALD to
372synthesize $\text{MoS}_2/\text{TiO}_2$ overlayers for photocathodes. Combining insights from
373electrochemical and spectroscopic characterization, we determined that: (1)
374 $\text{MoS}_2/\text{TiO}_2$ can serve as an effective catalytic scheme for CdS/CGSe
375photocathodes, (2) these overlayers provided only short-term protection
376from the acidic electrolyte, and (3) the degradation process is
377inhomogeneous and likely occurs through multiple pathways, ultimately
378exposing the underlying CGSe absorber. Building on these findings, the
379overlayer synthesis developed here can be further optimized and also
380generalized to other material systems that are constrained by sensitivity to
381temperature. Improvements in activity and durability for CdS/CGSe
382photocathodes would facilitate the development of promising tandem

383schemes for unassisted water splitting, and further work to disentangle the
384complex degradation pathways and interfacial energetics would accelerate
385such developments.

386

387**Acknowledgments**

388The work was funded by the Department of Energy (DOE) under contract no.
389DE-EE0006670, administrated by the University of Hawaii. This research
390used resources of the Advanced Light Source, which is a DOE Office of
391Science User Facility under contract no. DE-AC02-05CH11231. Fundamental
392catalyst development was supported by the U.S. Department of Energy,
393Chemical Sciences, Geosciences, and Biosciences (CSGB) Division of the
394Office of Basic Energy Sciences, via Grant DE-AC02-76SF00515 to the
395SUNCAT Center for Interface Science and Catalysis. Part of this work was
396performed at the Stanford Nano Shared Facilities (SNSF), supported by the
397National Science Foundation under award ECCS-1542152. Part of this work
398was also conducted at the Stanford Nanofabrication Facility (SNF) with
399guidance from their staff, especially Dr. Michelle Rincon. Thank you to Dr.
400Pongkarn Chakthranont for contributing the three-dimensional device
401schematic. Finally, TRH and DWP would like to thank the National Science
402Foundation for its support through the Graduate Research Fellowship
403Program.

404

405 *Supporting Information*. Additional details regarding calibration, data
406 analysis, and material synthesis and characterization can be found in the
407 *Supporting Information*.

408

409 **References**

410

4111. Häussinger, P.; Lohmüller, R.; Watson, A. M.. Hydrogen, 6. Uses. In
412 *Ullmann's Encyclopedia of Industrial Chemistry*, Wiley-VCH: Weinheim,
413 Germany, 2000.

4142. Badwal, S. P.; Giddey, S.; Munnings, C. Hydrogen production via solid
415 electrolytic routes. *Wiley Interdisciplinary Reviews: Energy and Environment*
416 **2013**, 2, 473-487.

4173. Kim, J. W.; Boo, K. J.; Cho, J. H.; Moon, I. 1 - Key challenges in the
418 development of an infrastructure for hydrogen production, delivery, storage
419 and use. In *Advances in Hydrogen Production, Storage and Distribution*;
420 Basile, A.; Iulianelli, A., Eds; Woodhead: Sawston, UK, 2014; pp 3-31.

4214. Bak, T.; Nowotny, J.; Rekas, M.; Sorrell, C. C. Photo-electrochemical
422 hydrogen generation from water using solar energy. Materials-related
423 aspects. *International Journal of Hydrogen Energy* **2002**, 27, 991-1022.

4245. Pinaud, B. A.; Benck, J. D.; Seitz, L. C.; Forman, A. J.; Chen, Z. B.;
425 Deutsch, T. G.; James, B. D.; Baum, K. N.; Baum, G. N.; Ardo, S.; Wang, H. L.;
426 Miller, E.; Jaramillo, T. F. Technical and economic feasibility of centralized
427 facilities for solar hydrogen production via photocatalysis and
428 photoelectrochemistry. *Energy & Environmental Science* **2013**, 6, 1983-
429 2002.

4306. Walter, M. G.; Warren, E. L.; McKone, J. R.; Boettcher, S. W.; Mi, Q. X.;
431 Santori, E. A.; Lewis, N. S. Solar Water Splitting Cells. *Chemical Reviews*
432 **2010**, 110, 6446-6473.

4337. Seitz, L. C.; Chen, Z.; Forman, A. J.; Pinaud, B. A.; Benck, J. D.; Jaramillo,
434 T. F. Modeling Practical Performance Limits of Photoelectrochemical Water
435 Splitting Based on the Current State of Materials Research. *ChemSusChem*
436 **2014**, 7, 1372-85.

4378. Hu, S.; Xiang, C. X.; Haussener, S.; Berger, A. D.; Lewis, N. S. An
438 analysis of the optimal band gaps of light absorbers in integrated tandem
439 photoelectrochemical water-splitting systems. *Energy & Environmental*
440 *Science* **2013**, 6, 2984-2993.

4419. Weber, M. F.; Dignam, M. J. Efficiency of Splitting Water with
442 Semiconducting Photoelectrodes. *Journal of the Electrochemical Society*
443 **1984**, 131, 1258-1265.

44410. Doscher, H.; Geisz, J. F.; Deutsch, T. G.; Turner, J. A. Sunlight
445 absorption in water—efficiency and design implications for

446 photoelectrochemical devices. *Energy & Environmental Science* **2014**, *7*, 4472951-2956.

44811. Shaner, M. R.; Atwater, H. A.; Lewis, N. S.; McFarland, E. W. A
449 comparative technoeconomic analysis of renewable hydrogen production
450 using solar energy. *Energy & Environmental Science* **2016**, *9*, 2354-2371.

45112. Young, D. L.; Keane, J.; Duda, A.; AbuShama, J. A.; Perkins, C. L.;
452 Romero, M.; Noufi, R. Improved performance in ZnO/CdS/CuGaSe₂ thin-film
453 solar cells. *Progress in Photovoltaics: Research and Applications* **2003**, *11*,
454 535-541.

45513. Powalla, M.; Witte, W.; Jackson, P.; Paetel, S.; Lotter, E.; Wuerz, R.;
456 Kessler, F.; Tschamber, C.; Hempel, W.; Hariskos, D.; Menner, R.; Bauer, A.;
457 Spiering, S.; Ahlswede, E.; Friedlmeier, T. M.; Blázquez-Sánchez, D.; Klugius,
458 I.; Wischmann, W. CIGS Cells and Modules with High Efficiency on Glass and
459 Flexible Substrates. *IEEE Journal of Photovoltaics* **2014**, *4*, 440-446.

46014. Panthani, M. G.; Akhavan, V.; Goodfellow, B.; Schmidtke, J. P.; Dunn, L.;
461 Dodabalapur, A.; Barbara, P. F.; Korgel, B. A. Synthesis of CuInS₂, CuInSe₂,
462 and Cu(In_xGa_{1-x})Se₂ (CIGS) Nanocrystal 'Inks' for Printable Photovoltaics.
463 *Journal of the American Chemical Society* **2008**, *130*, 16770-16777.

46415. Uhl, A. R.; Katahara, J. K.; Hillhouse, H. W. Molecular-ink route to 13.0%
465 efficient low-bandgap CuIn(S,Se)₂ and 14.7% efficient Cu(In,Ga)(S,Se)₂ solar
466 cells. *Energy & Environmental Science* **2016**, *9*, 130-134.

46716. Bär, M.; Bohne, W.; Röhrich, J.; Strub, E.; Lindner, S.; Lux-Steiner, M. C.;
468 Fischer, C.-H.; Niesen, T. P.; Karg, F. Determination of the band gap depth
469 profile of the pentenary Cu(In_(1-x)Ga_x(S_ySe_(1-y))₂ chalcopyrite from its
470 composition gradient. *Journal of Applied Physics* **2004**, *96*, 3857-3860.

47117. Kumagai, H.; Minegishi, T.; Moriya, Y.; Kubota, J.; Domen, K.
472 Photoelectrochemical Hydrogen Evolution from Water Using Copper Gallium
473 Selenide Electrodes Prepared by a Particle Transfer Method. *The Journal of*
474 *Physical Chemistry C* **2014**, *118*, 16386-16392.

47518. Moriya, M.; Minegishi, T.; Kumagai, H.; Katayama, M.; Kubota, J.;
476 Domen, K. Stable Hydrogen Evolution from CdS-Modified CuGaSe₂
477 Photoelectrode under Visible-Light Irradiation. *Journal of the American*
478 *Chemical Society* **2013**, *135*, 3733-3735.

47919. Marsen, B.; Cole, B.; Miller, E. L. Photoelectrolysis of water using thin
480 copper gallium diselenide electrodes. *Solar Energy Materials and Solar Cells*
481 **2008**, *92*, 1054-1058.

48220. Kaneshiro, J.; Gaillard, N.; Rocheleau, R.; Miller, E. Advances in copper-
483 chalcopyrite thin films for solar energy conversion. *Solar Energy Materials*
484 *and Solar Cells* **2010**, *94*, 12-16.

48521. Naghavi, N.; Abou-Ras, D.; Allsop, N.; Barreau, N.; Bücheler, S.;
486 Ennaoui, A.; Fischer, C. H.; Guillen, C.; Hariskos, D.; Herrero, J. Buffer layers
487 and transparent conducting oxides for chalcopyrite Cu(In,Ga)(S,Se)₂ based
488 thin film photovoltaics: present status and current developments. *Progress in*
489 *Photovoltaics: Research and Applications* **2010**, *18*, 411-433.

49022. Inoue, T.; Watanabe, T.; Fujishima, A.; Honda, K. i.; Kohayakawa, K.
491Suppression of surface dissolution of CdS photoanode by reducing agents.
492*Journal of The Electrochemical Society* **1977**, *124*, 719-722.

49323. Gerischer, H. On the stability of semiconductor electrodes against
494photodecomposition. *Journal of Electroanalytical Chemistry and Interfacial*
495*Electrochemistry* **1977**, *82*, 133-143.

49624. Jin, J.; Walczak, K.; Singh, M. R.; Karp, C.; Lewis, N. S.; Xiang, C. X. An
497experimental and modeling/simulation-based evaluation of the efficiency and
498operational performance characteristics of an integrated, membrane-free,
499neutral pH solar-driven water-splitting system. *Energy & Environmental*
500*Science* **2014**, *7*, 3371-3380.

50125. Benck, J. D.; Lee, S. C.; Fong, K. D.; Kibsgaard, J.; Sinclair, R.; Jaramillo,
502T. F. Designing Active and Atable Silicon Photocathodes for Solar Hydrogen
503Production Using Molybdenum Sulfide Nanomaterials. *Advanced Energy*
504*Materials* **2014**, *4*, 1400739.

50526. Britto, R. J.; Benck, J. D.; Young, J. L.; Hahn, C.; Deutsch, T. G.; Jaramillo,
506T. F. Molybdenum Disulfide as a Protection Layer and Catalyst for Gallium
507Indium Phosphide Solar Water Splitting Photocathodes. *The Journal of*
508*Physical Chemistry Letters* **2016**, *7*, 2044-2049.

50927. Gu, J.; Aguiar, J. A.; Ferrere, S.; Steirer, K. X.; Yan, Y.; Xiao, C.; Young,
510James L.; Al-Jassim, M.; Neale, N. R.; Turner, J. A. A graded catalytic-
511protective layer for an efficient and stable water-splitting photocathode.
512*Nature Energy* **2017**, *2*, 16192.

51328. King, L. A.; Hellstern, T. R.; Park, J.; Sinclair, R.; Jaramillo, T. F. Highly
514Stable Molybdenum Disulfide Protected Silicon Photocathodes for
515Photoelectrochemical Water Splitting. *ACS Appl. Mater. Interfaces* **2017**, *9*,
51636792-36798.

51729. Morales-Guio, C. G.; Tilley, S. D.; Vrubel, H.; Grätzel, M.; Hu, X.
518"Hydrogen evolution from a copper (I) oxide photocathode coated with and
519amorphous molybdenum sulphide catalyst" *Nature Communications* **2014**,
5205, 3059.

52130. Laursen, A. B.; Pedersen, T.; Malacrida, P.; Seger, B.; Hansen, O.;
522Vesborg, P. C. K.; Chorkendorff, I. MoS₂—an integrated protective and active
523layer on n⁺p-Si for solar H₂ evolution. *Phys. Chem. Chem. Phys.* **2013**, *15*,
52420000-20004.

52531. Benck, J. D.; Hellstern, T. R.; Kibsgaard, J.; Chakthranont, P.; Jaramillo,
526T. F. Catalyzing the Hydrogen Evolution Reaction (HER) with Molybdenum
527Sulfide Nanomaterials. *ACS Catalysis* **2014**, *4*, 3957-3971.

52832. Jaramillo, T. F.; Jørgensen, K. P.; Bonde, J.; Nielsen, J. H.; Horch, S.;
529Chorkendorff, I. Identification of Active Edge Sites for Electrochemical H₂
530Evolution from MoS₂ Nanocatalysts. *Science* **2007**, *317*, 100-102.

53133. Contreras, M. A.; Tuttle, J.; Gabor, A.; Tennant, A.; Ramanathan, K.;
532Asher, S.; Franz, A.; Keane, J.; Wang, L.; Scofield, J.; Noufi, R. High Efficiency
533Cu(In,Ga)Se₂-Based Solar Cells: Processing of Novel Absorber Structures.
534*Proceedings of 1994 IEEE 1st World Conference on Photovoltaic Energy*
535*Conversion*. **1994**, *1*, 68-75.

53634. DeAngelis, A. D.; Horsley, K.; Gaillard, N. Wide Band Gap CuGa(S,Se)₂
537Thin Films on Transparent Conductive Fluorinated Tin Oxide Substrates as
538Photocathode Candidates for Tandem Water Splitting Devices. *J. Phys. Chem.*
539C **2018**, *122*, 14304-14312.

54035. Hu, S.; Shaner, M. R.; Beardslee, J. A.; Lichterman, M.; Brunschwig, B.
541S.; Lewis, N. S. Amorphous TiO₂ coatings stabilize Si, GaAs, and GaP
542photoanodes for efficient water oxidation. *Science* **2014**, *344*, 1005-1009.

54336. Diskus, M.; Nilsen, O.; Fjellvag, H. Growth of thin films of molybdenum
544oxide by atomic layer deposition. *J. Mater. Chem.* **2011**, *21*, 705-710.

54537. Chen, Z.; Cummins, D.; Reinecke, B. N.; Clark, E.; Sunkara, M. K.;
546Jaramillo, T. F. Core-shell MoO₃-MoS₂ Nanowires for Hydrogen Evolution: A
547Functional Design for Electrocatalytic Materials. *Nano Letters* **2011**, *11*,
5484168-4175.

54938. Qiao, R.; Li, Q.; Zhuo, Z.; Sallis, S.; Fuchs, O.; Blum, M.; Weinhardt, L.;
550Heske, C.; Pepper, J.; Jones, M.; Brown, A.; Spucce, A.; Chow, K.; Smith, B.;
551Glans, P.-A.; Chen, Y.; Yan, S.; Pan, F.; Piper, L. F. J.; Denlinger, J.; Guo, J.;
552Hussain, Z.; Chuang, Y.-D.; Yang, W. High-efficiency *in situ* resonant inelastic
553x-ray scattering (iRIXS) endstation at the Advanced Light Source. *Review of*
554*Scientific Instruments* **2017**, *88*, 033106.

55539. Chen, Z.; Jaramillo, T. F.; Deutsch, T. G.; Kleiman-Schwarzstein, A.;
556Forman, A. J.; Gaillard, N.; Garland, R.; Takanabe, K.; Heske, C.; Sunkara, M.;
557McFarland, E. W.; Domen, K.; Miller, E. L.; Turner, J. A.; Dinh, H. N.
558Accelerating materials development for photoelectrochemical hydrogen
559production: Standards for methods, definitions, and reporting protocols. *J.*
560*Mater. Res.* **2010**, *25*, 3-16.

56140. Poortmans, J.; Arkhipov, V., *Thin film solar cells: fabrication,*
562*characterization and applications.* Wiley: New York, 2006.

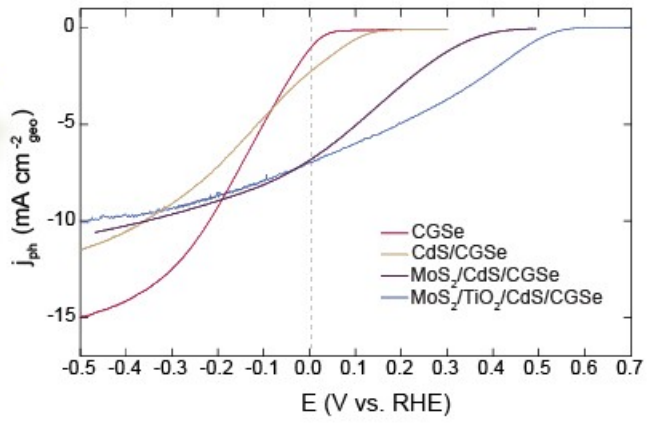
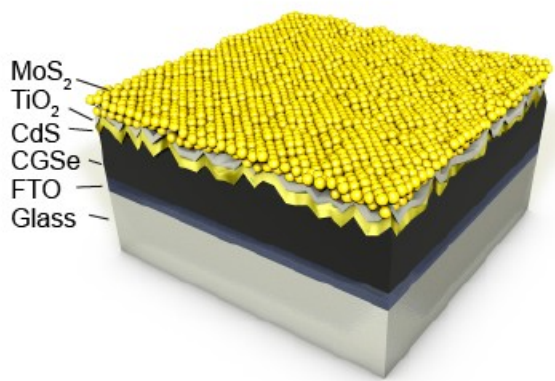
56341. Weinhardt, L.; Fuchs, O.; Fleszar, A.; Bär, M.; Blum, M.; Weigand, M.;
564Denlinger, J. D.; Yang, W.; Hanke, W.; Umbach, E.; Heske, C. Resonant
565inelastic soft x-ray scattering of CdS: A two-dimensional electronic structure
566map approach. *Physical Review B* **2009**, *79*, 165305.

56742. Weinhardt, L.; Fuchs, O.; Umbach, E.; Heske, C.; Fleszar, A.; Hanke, W.;
568Denlinger, J. D. Resonant inelastic soft x-ray scattering, x-ray absorption
569spectroscopy, and density functional theory calculations of the electronic
570bulk band structure of CdS. *Physical Review B* **2007**, *75*, 165207.

57143. Pookpanratana, S.; Repins, I.; Bär, M.; Weinhardt, L.; Zhang, Y.; Félix,
572R.; Blum, M.; Yang, W.; Heske, C. CdS/Cu(In,Ga)Se₂ interface formation in
573high-efficiency thin film solar cells. *Applied Physics Letters* **2010**, *97*,
574074101.

575
576

577Table of Contents Graphic



578